An overlap expansion method for improving ab initio model potentials: Anisotropic intermolecular potentials of N2, CO, and C2H2 with He*(2 3S)

doi: 10.1063/1.1630954

An overlap expansion method for improving *ab initio* model potentials: Anisotropic intermolecular potentials of N_2, CO, and C_2H_2 with He*($2\,^3S$)

Satoshi Maeda, Masakazu Yamazaki, Naoki Kishimoto, and Koichi Ohno[a)]
Department of Chemistry, Graduate School of Science, Tohoku University, Aramaki, Aoba-ku, Sendai 980-8578, Japan

(Received 22 September 2003; accepted 14 October 2003)

An overlap expansion method is proposed for improving *ab initio* model potentials. Correction terms are expanded in terms of overlap integrals between orbitals of the interacting system. The method is used to improve *ab initio* model potentials for $N_2+He^*(2\,^3S)$, $CO+He^*(2\,^3S)$, and $C_2H_2+He^*(2\,^3S)$. Physical meanings of the optimization are elucidated in terms of target orbitals. Correction terms are found to be dominated by the components of HOMO, LUMO, next-HOMO, and next-LUMO on the target molecule. The present overlap expansion method using a limited number of correction terms related to frontier orbitals provides an efficient and intuitive approach for construction of highly anisotropic intermolecular interaction potentials. © *2004 American Institute of Physics.* [DOI: 10.1063/1.1630954]

I. INTRODUCTION

In order to elucidate chemical reaction dynamics and intermolecular interactions, potential energy surfaces (PES) should be determined in good accuracy.[1–5] Although quantum chemical methods have been developed extensively, calculated PES often need to be improved with the aid of experimental data, especially for intermolecular potentials. Various expansion techniques using many correction terms often undergo slow convergence or sever indeterminacy. Even if interaction potentials could be improved by many correction terms, physical significance of the corrections has often been disregarded. Thus, the lack of efficient and intuitive potential correction techniques has been an obstacle for many investigations concerning PES. In this regard, comparative studies connecting theory and experiment need to be made in detail.

One of the simplest reaction processes including atom–molecule interactions, which can be treated in sufficient levels of both theory and experiment, is a collisional ionization known as Penning ionization,[6] an ionization process of a molecule M by collision with a metastable atom A*, such as $He^*(2\,^3S)$, having an excitation energy larger than the lowest ionization potential (IP) of the molecule,

$$A^*+M\rightarrow A+M_i^+ +e^-. \tag{1}$$

According to the electron exchange mechanism of Penning ionization,[7] ionization by $He^*(2\,^3S)$ takes place with a high probability when the He 1*s* orbital overlaps effectively with the molecular orbital from which an electron is removed. The relative collision energy E_c is one of the important variables, because collision trajectories causing effective overlaps between the orbitals depend on E_c. The cross sections then may either increase or decrease with an increase of the E_c depending on the trajectories influenced by intermolecular interactions.[8] Coupled experimental techniques including velocity selection and electron kinetic energy analysis of Penning ionization have been developed.[9–15] Recently, these techniques further developed to give collision energy/electron energy resolved two-dimensional Penning ionization electron spectra (2D-PIES),[16] from which we can obtain (a) collision energy resolved Penning ionization electron spectra (CERPIES) and (b) collision energy dependence of partial Penning ionization cross sections (CEDPICS) for all final ionic states. For molecular targets, each CEDPICS for a particular final ionic state reflects the interaction potential in the region where the corresponding molecular orbital extends, therefore anisotropy of interaction potentials between molecules and excited atoms can be studied from CEDPICS.

Theories of Penning ionization have been established by Nakamura[17] and Miller.[18] The collision dynamics in Penning ionization have been studied mainly for atomic targets[17–22] and simple molecules such as H_2[23,24] and N_2[25–27] because of the difficulties to obtain accurate PES and ionization widths by *ab initio* calculations. Ishida and Horime[26,27] have performed pioneering calculations of CEDPICS for $N_2+He^*(2\,^3S)$ by using various approximations based on *ab initio* potentials;[28] PES for the excited state was obtained directly, but employed basis sets were limited. Ogawa *et al.*[29] performed classical trajectory calculations for $N_2+He^*(2\,^3S)$ by using the Li model potential of $N_2+Li(2\,^2S)$ based on the similarity between $He^*(2\,^3S)$ and $Li(2\,^2S)$ in an interaction with various atomic targets.[30–35] The Li model potential optimized by simple scaling[29] has been successful in reproducing the slope of observed CEDPICS, although the branching ratios were not optimized. Branching ratios as well as the slopes of CEDPICS have first been reproduced by trajectory calculations of 2D-PIES for $N_2+He^*(2\,^3S)$.[36] Classical trajectory calculations of 2D-PIES for $CO+He^*(2\,^3S)$ were also performed,[37] where the calculated slopes of CEDPICS was found to be less reliable than the case of $N_2+He^*(2\,^3S)$. Recently, the exponential correction (EC) method was developed to improve *ab initio*

a)Electronic mail: ohnok@qpcrkk.chem.tohoku.ac.jp

Li model potentials and applied to $N_2+He^*(2\,^3S)$ and $CO+He^*(2\,^3S)$ systems.[38,39]

Although *ab initio* model potentials using a Li atom in place of a $He^*(2\,^3S)$ atom have been optimized to give satisfactory results in the scheme of the EC method, physical significance of the optimization has not yet been elucidated. In addition to this, the EC method has a serious problem, when it is applied to a large molecule. The one-center Legendre expansion used in the EC method is not appropriate for large nonlinear molecules such as benzene. A brute-force approach using expansions up to very high orders should be prohibited, because of the following reasons; the increase of the number of expansion coefficients makes unable to extract physical significance, and the optimization process tends to undergo very slow convergence with considerable ambiguities caused by many parameters.

Since linear combinations of atomic orbitals have been used extensively and successfully in quantum chemical problems rather than one-center expansion techniques, correction and construction of intermolecular potentials can also be made in terms of chemical components. It is of note that intermolecular interactions are in most cases fundamentally related to (a) overlap integrals between the interacting species and (b) limited numbers of orbitals such as the highest molecular orbital (HOMO) and the lowest unoccupied molecular orbital (LUMO). Therefore, it is interesting to expand interaction potentials in terms of overlap integrals related to some important molecular orbitals.

In this study, an overlap expansion (OE) method is proposed for improving *ab initio* model potentials. In the OE method, correction terms are expanded in terms of overlap integrals between the *s* orbital of a He* atom and target valence molecular orbitals. The OE method is used to improve *ab initio* Li model potentials for $N_2+He^*(2\,^3S)$, $CO+He^*(2\,^3S)$, and $C_2H_2+He^*(2\,^3S)$ systems, and results are compared with other methods. The OE method has advantages in disclosing physical meanings of the optimization in terms of target molecular orbitals such as HOMO and LUMO as well as further applications to the larger systems.

II. CALCULATIONS

A. *Ab initio* Li model potential

In order to avoid difficulties associated with highly excited electronic states embedded in ionization continua, we can start from an approximate potential (Li model potential) using a Li $(2\,^2S)$ atom in place of a $He^*(2\,^3S)$ atom, based on the well known similarity between $He^*(2\,^3S)$ and Li $(2\,^2S)$ atoms.[30–35] The Li model potential V_0 for interactions between the target molecule M and a Li atom can be expressed by the following equation:

$$V_0 = E_{\mathrm{MLi}} - (E_{\mathrm{M}} + E_{\mathrm{Li}}). \tag{2}$$

Here E_{MLi}, E_{M}, and E_{Li} are the energy of the interacting system M+Li, the isolated molecule M, and the isolated Li atom, respectively.

E_{MLi} and E_{M} were obtained by the coupled cluster method including single, double, and optional triple excitation CCSD(T), and E_{Li} was calculated by use of the unrestricted Hartree–Fock method. 6-311+G* basis sets were employed for N_2+Li and CO+Li, and 6-311++G** basis sets were used in the case of C_2H_2+Li. The experimental equilibrium structure in the ground state was used for each molecule. A full counterpoise method[40] was employed to correct the basis set superposition error. *Ab initio* energy calculations were carried out by use of GAUSSIAN 94 programs.[41]

B. Simple scaling (SS) method and exponential correction (EC) method

In order to improve *ab initio* Li model potentials V_0 by optimization procedures using an experimental 2D-PIES, a simple scaling method[29,36,37] and an exponential correction method[38,39] have been employed.

The simple scaling (SS) model potential V_{SS} is expressed as

$$V_{\mathrm{SS}} = a \cdot V_0. \tag{3}$$

Here, scaling constant a is a parameter, which is introduced to improve an overestimation of repulsive interactions or the deficiency of electron correlation effects. This method is, however, not able to be used for systems with attractive potential wells, because modifications in the positive parts and the negative parts are not compatible. Moreover, the constant scaling is not suitable to improve strongly anisotropic potentials.

The exponential correction (EC) method has been designed to be applied for both attractive and repulsive parts of potentials by using exponential functions for the radial parts in combination with Legendre expansions for the anisotropic angular parts. Corrected potentials of V_{EC} in the EC method are expressed as follows:

$$V_{\mathrm{EC}}(R,\theta) = V_0(R,\theta) - \sum_{i=0-4} A_i P_i(\cos\theta)\exp(-R/B). \tag{4}$$

Here, R is the distance between the He*(Li) atom and the center of mass of the molecule, θ denotes the angle of the vector **R** directing to the He*(Li) atom from the center of mass with respect to the molecular axis, $P_i(\cos\theta)$ is the ith order term of Legendre polynomials, and A_i and B are parameters to be optimized. In Eq. (4), the anisotropy of the interactions can be modified by the Legendre expansion parameters A_i, and the radial dependence of the interactions can be changed by the parameter B.

C. Overlap expansion (OE) method

In the present study, the overlap expansion (OE) method was introduced to modify V_0 more efficiently by using quantum chemical characteristics of the target molecule. The OE model potential V_{OE} is expressed as

$$V_{\mathrm{OE}}(R,\theta) = V_0(R,\theta) - \sum_i C_i |\langle \phi_i | \chi \rangle|^2, \tag{5}$$

$$\chi = \sqrt{\zeta^3/\pi}\exp[-\zeta r]. \tag{6}$$

Here, R is the distance of the He*(Li) atom from the center of mass of the molecule, θ denotes the angle of the position

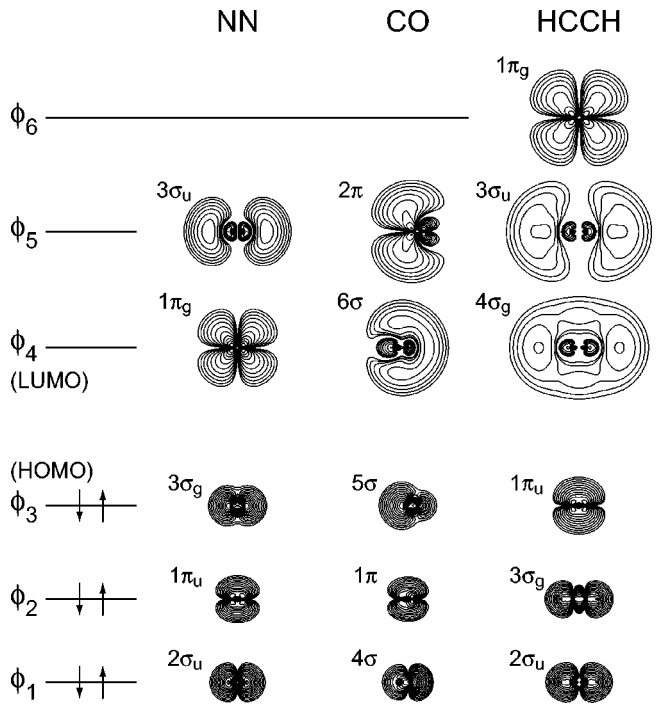

FIG. 1. Molecular orbitals of isoelectronic molecules of N_2, CO, and C_2H_2. Electron density maps are drawn in a common scale. Atomic positions are from the left to the right, NN, CO, and HCCH, respectively. $\phi_1 \sim \phi_3$ are occupied molecular orbitals, and ϕ_3 is the highest occupied molecular orbitals (HOMO). $\phi_4 \sim \phi_6$ are unoccupied molecular orbitals, and ϕ_4 is the lowest unoccupied molecular orbitals (LUMO). ϕ_6 for N_2 and CO are omitted because they are outside the valence shell. The numberings of the orbitals are in common with those in Table IV.

vector **R** directing to the He*(Li) atom from the center of mass with respect to the molecular axis. ϕ_i is the target molecular orbital. χ is a Slater type *s* orbital function with an exponent ζ, which is placed at the position of He*(Li) atom. *r* is the distance from the center of χ. The OE method is designed to describe anisotropic interactions by expanded terms using overlap integrals between molecular orbitals ϕ_i and an atomic orbital χ. The expansion coefficients C_i and the atomic orbital exponent ζ are parameters for the optimization.

The range of the expansion for the target orbitals ϕ_i may be chosen from the following criteria. (a) Although the mathematical flexibility requires many functions in the expansion, number of variable parameters should be suppressed as small as possible in order to avoid the indeterminacy in the optimization and too heavy computational demands. (b) Meaningful interactions are expected to be concentrated in valence molecular orbitals, especially higher occupied orbitals and lower unoccupied orbitals.

Considering these factors, molecular orbitals in the expansion were limited to valence molecular orbitals. In trial calculations, inner valence orbitals with large $2s$ characters were found to be unimportant, and the highest unoccupied valence orbital of C_2H_2 could be disregarded. Thus, the following molecular orbitals are only retained in the present study; $2\sigma_u$, $1\pi_u$, $3\sigma_g$, $1\pi_g$, and $3\sigma_u$ orbitals for N_2, 4σ, 1π, 5σ, 6σ, and 2π orbitals for CO, and $2\sigma_u$, $3\sigma_g$, $1\pi_u$, $4\sigma_g$, $3\sigma_u$, and $1\pi_g$ orbitals for C_2H_2. Figure 1 shows these orbitals, which indicates the numbering of ϕ_i and C_i for each system. In Fig. 1, HOMO denotes the highest occupied molecular orbital, and LUMO denotes the lowest unoccupied molecular orbital. These molecular orbitals are those obtained by HF/6-311+G* and HF/6-311++G** levels of calculations.

D. Classical trajectory calculations

Classical trajectory calculations obtaining collision energy dependence of partial ionization cross sections (CEDPICS) need to be made for each potential energy function of the interacting systems. Classical trajectories of the He* atom with respect to the molecule were determined by solving the equation of motion. For various collision energies, a number of trajectories were considered for randomly generated initial conditions, such as impact parameters, molecular orientation, and angular momenta.

In each trajectory step, transition probabilities $P^{(i)}(t)dt$ into each ionic state *i* were calculated by

$$P^{(i)}(t)dt = S(t)\frac{\Gamma^{(i)}}{\hbar}dt, \tag{7}$$

$$\Gamma^{(i)} = K^{(i)}|\langle \phi_i|\psi_{1s}\rangle|^2, \tag{8}$$

$$S(t) = 1 - \sum_i P^{(i)}_{\text{int}}(t), \tag{9}$$

where $\Gamma^{(i)}$ is the ionization width for transition to the *i*th ionic state, which is a function of the position vector **R** directing to the He*(Li) atom from the center of mass of the target molecule. An overlap method in Eq. (8) is employed in order to avoid the following difficulties; (a) theoretical difficulties associated with direct calculations of the matrix elements, including very high excited states, and (b) computational difficulties associated with too many geometrical configurations and two electron integrals. Theoretical features of this overlap method for the estimation of ionization widths have been described in detail in the previous paper.[39] ϕ_i and ψ_{1s} are the ionized orbital of the target molecule and the $1s$ orbital of the He atom, respectively. $K^{(i)}$ is a parameter for each ionic state to be determined so as to reproduce observed ionization branching ratios, which can be obtained from the relative band intensities in 2D-PIES. The survival fraction $S(t)$ represents the survival probability of He* in the excited state at a certain time *t*. After calculations of 10000 trajectories with various impact parameters, the partial ionization cross section $\sigma^{(i)}$ was obtained from the ionization probability $P^{(i)}$ with a weight of $2\pi b db$,

$$\sigma^{(i)} = \int_0^\infty 2\pi b P^{(i)} db. \tag{10}$$

E. Optimization of parameters

Parameters for correction terms in Eqs. (4), (5), and (6) as well as $K^{(i)}$ in Eq. (8) were optimized by a nonlinear least square fitting method, so as to reproduce observed slopes in CEDPICS and observed branching ratios in 2D-PIES. In each iteration, the optimization step was obtained by the modified Marquardt method.[42] The gradient vector and the

TABLE I. The slopes m of the $\log\sigma$–$\log E_c$ plots in CEDPICS.

System	Ionic states	Collision energy/meV	Obs.	Calc.[c] (V_{SS})	Calc. (V_{EC})	Calc.[f] (V_{OE})
N_2/He*($2\,^3S$)	$X\,^2\Sigma_g^+$	100–200	0.68[a]	0.85	0.65[d]	0.67
		200–300	0.36[a]	0.45	0.41[d]	0.24
	$A\,^2\Pi_u$	100–200	1.08[a]	1.38	1.14[d]	1.19
		200–300	0.52[a]	0.87	0.79[d]	0.59
	$B\,^2\Sigma_u^+$	100–200	0.66[a]	0.84	0.69[d]	0.73
		200–300	0.28[a]	0.50	0.47[d]	0.27
CO/He*($2\,^3S$)	$X\,^2\Sigma^+$	100–200	0.17[a]	0.45	0.17[d]	0.24
		200–300	0.08[a]	0.31	0.12[d]	0.01
	$A\,^2\Pi$	100–200	0.74[a]	1.15	0.83[d]	0.79
		200–300	0.52[a]	0.65	0.40[d]	0.44
	$B\,^2\Sigma^+$	100–200	0.49[a]	0.83	0.58[d]	0.52
		200–300	0.32[a]	0.38	0.28[d]	0.23
C_2H_2/He*($2\,^3S$)	$X\,^2\Pi_u$	100–200	−0.23[b]	—	−0.20[e]	−0.24
		200–300	−0.17[b]	—	−0.07[e]	−0.24
	$A\,^2\Sigma_g^+$	100–200	0.09[b]	—	0.15[e]	0.12
		200–300	0.15[b]	—	0.16[e]	0.13
	$B\,^2\Sigma_u^+$	100–200	0.10[b]	—	0.20[e]	0.12
		200–300	0.26[b]	—	0.19[e]	0.14

[a]2D-PIES experiments in Ref. 44 for N_2/He*($2\,^3S$) and Ref. 37 for CO/He*($2\,^3S$).
[b]The present 2D-PIES experiments.
[c]The previous calculations by the simple scaling model potentials V_{SS} in Ref. 38 for N_2/He*($2\,^3S$) and CO/He*($2\,^3S$).
[d]The previous calculations by the exponential correction model potentials V_{EC} in Ref. 38 for N_2/He*($2\,^3S$) and CO/He*($2\,^3S$).
[e]The present calculations by the exponential correction model potentials V_{EC}.
[f]The present calculations by the overlap expansion model potentials V_{OE}.

Hessian matrix for obtaining a Marquardt step were calculated numerically only in the first iteration, and then they were updated based on the hybrid method proposed by Powell.[43]

III. EXPERIMENT SECTION

In order to optimize potentials functions for fitting with experimental data, we used observed 2D-PIES of $N_2+He^*(2\,^3S)$,[39,44] $CO+He^*(2\,^3S)$,[37,39] and $C_2H_2+He^*(2\,^3S)$. 2D-PIES data for $C_2H_2+He^*(2\,^3S)$ were newly measured in the present study.

The experimental apparatus has been reported in previous papers.[9–12,16] A metastable beam of He was produced by a nozzle discharge source, and the $He^*(2\,^1S)$ component was quenched by a water-cooled helium discharge lamp. The metastable $He^*(2\,^3S)$ beam was pulsed by a mechanical chopper and then introduced into a collision cell located 504 mm downstream from the chopper disk. The kinetic energy of electrons was measured by a hemispherical electrostatic deflection type analyzer using an electron collection angle 90° to the incident $He^*(2\,^3S)$ beam. The transmission efficiency curve of the electron energy analyzer was determined by comparing our HeI UPS data with those of Gardner and Samson[45] and Kimura *et al.*[46] The energy resolution of the electron energy analyzer was 70 meV estimated from the full width at half maximum (fwhm) of the $Ar^+(^2P_{3/2})$ peak in the HeI UPS.

The He* velocity distribution $I_{He^*}(\nu_{He^*})$ was obtained by measuring a time-of-flight (TOF) of electrons emitted from a stainless steel plate inserted into the collision cell, because the TOF of secondary electrons from the metal surface to the detector is negligibly short in comparison with that of the He* atoms. The 2D-PIES intensity of sample molecules $I_e(E_e,t)$ as functions of electron kinetic energy E_e and time t was converted to $I_e(E_e,\tau_{TOF})$ as functions of E_e and TOF of the He* beam. The $I_e(E_e,\tau_{TOF})$ can lead to $I_e(E_e,\nu_{He^*})$ as functions of E_e and velocity of He* atoms ν_{He^*}. By the following equations, the 2D Penning ionization cross section $\sigma(E_e,\nu_r)$ was obtained:

$$\sigma(E_e,\nu_r)=c\,\frac{I_e(E_e,\nu_{He^*})}{I_{He^*}(\nu_{He^*})}\,\frac{\nu_{He^*}}{\nu_r}, \tag{11}$$

$$\nu_r=\sqrt{\nu_{He^*}^2+\frac{3k_BT}{m}}, \tag{12}$$

where c is a constant, ν_r is the relative velocity averaged over the velocity of the target molecule, k_B is the Boltzmann constant, and T and m are the gas temperature and the mass of the target molecule, respectively. The cross section in Eq. (11) is normalized with the velocity distribution $I_{He^*}(\nu_{He^*})$ of the He* beam. $\sigma(E_e,\nu_r)$ is converted to $\sigma(E_e,E_c)$ by the relation

$$E_c=\tfrac{1}{2}\mu\nu_r^2, \tag{13}$$

where μ is the reduced mass of the colliding system.

IV. RESULTS

Table I lists observed slopes m of $\log\sigma^{(i)}$–$\log E_c$ plots for X, A, and B ionic states in the energy regions of 100–200 meV and 200–300 meV for $N_2+He^*(2\,^3S)$, CO

TABLE II. The optimized parameters for the simple scaling model potential V_{SS} in Eq. (3) as well as $K^{(i)}$ in Eq. (8) for N_2/He*($2\,^3S$) and CO/He*($2\,^3S$), these are reported in Refs. 36 and 37, respectively.

	N_2/He*($2\,^3S$)	CO/He*($2\,^3S$)
a	0.80	0.55
$K^{(B)}$/eV	22.7	4.85
$K^{(A)}$/eV	16.6	5.66
$K^{(X)}$/eV	9.36	1.85

$+$He*($2\,^3S$), and C_2H_2+He*($2\,^3S$) in comparison with those obtained by the trajectory calculations with optimized potentials, V_{SS}, V_{EC}, and V_{OE}.

The optimized parameter values for the SS and EC methods are listed in Table II and Table III in order to compare them with those for the present OE method listed in Table IV. Obtained parameters for potential wells, the depth (D_e), the distance (R_e), and the angle (θ_e), are also listed in Table III and Table IV. Uncertainties of the potential parameters were estimated from errors of experimental slope values ($\Delta m = \pm 0.01$), and they are shown in parentheses.

Figure 2–4 show (a) a contour map of V_{OE} and (b) interaction potential curves of V_0 (dotted line), V_{EC} (broken line), and V_{OE} (solid line) for N_2+He*($2\,^3S$), CO $+$He*($2\,^3S$), and C_2H_2+He*($2\,^3S$), respectively. The spacing of the counter lines is 100 meV for positive values between 0 and 800 meV for each system, and 20 meV for negative values between -40 meV and 0 meV for the C_2H_2+He*($2\,^3S$) system. Figure 5 shows $\log\sigma^{(i)}$–$\log E_c$ plots of CEDPICS for (a) N_2+He*($2\,^3S$) and (b) CO $+$He*($2\,^3S$), respectively. Figure 6 shows $\log\sigma^{(i)}$–$\log E_c$ plots of CEDPICS for C_2H_2+He*($2\,^3S$).

Observed partial cross sections together with their total are shown with open circles. Observed data for N_2[39,44] and CO[37,39] were previously recorded, and the observed data for C_2H_2 were newly measured in the present study. Respective ionic states are $X\,^2\Sigma_g^+$, $A\,^2\Pi_u$, $B\,^2\Sigma_u^+$ for N_2, $X\,^2\Sigma^+$, $A\,^2\Pi$, $B\,^2\Sigma^+$ for CO, and $X\,^2\Pi_u$, $A\,^2\Sigma_g^+$, $B\,^2\Sigma_u^+$ for C_2H_2,

TABLE III. The optimized parameters for exponential correction model potential V_{EC} in Eq. (4) as well as $K^{(i)}$ in Eq. (8), obtained potential well depth D_e, and their positions R_e and θ_e, for N_2/He*($2\,^3S$), CO/He*($2\,^3S$), and C_2H_2/He*($2\,^3S$). Uncertainties for V_{EC} estimated from errors of experimental slope values ($\Delta m = \pm 0.01$) are shown in parentheses.

	N_2/He*($2\,^3S$)[a]	CO/He*($2\,^3S$)[a]	C_2H_2/He*($2\,^3S$)[b]
B_0/Å	1.104 ($\pm$0.014)	0.861 ($\pm$0.009)	1.535 ($\pm$0.049)
A_0/meV	941 ($\pm$5)	2870 ($\pm$3)	265 ($\pm$17)
A_1/meV	—	296 ($\pm$4)	—
A_2/meV	-379 ($\pm$7)	-1300 ($\pm$4)	56 ($\pm$57)
A_4/meV	0 ($\pm$7)	—	-146 ($\pm$974)
$K^{(B)}$/eV	13.6	4.23	87.9
$K^{(A)}$/eV	7.58	3.43	90.3
$K^{(X)}$/eV	5.71	1.66	7.54
D_e/meV	-9.22	-11.5	-26.6
R_e/Å	4.88	4.55	2.63
θ_e/degree	90.0	80.3	90.0

[a]The previous calculations reported in Ref. 38.
[b]The present calculations.

TABLE IV. The optimized parameters for present overlap expansion model potential V_{OE} in Eqs. (5) and (6) as well as $K^{(i)}$ in Eq. (8), obtained potential well depth D_e, and their positions R_e and θ_e, for N_2/He*($2\,^3S$), CO/He*($2\,^3S$), and C_2H_2/He*($2\,^3S$). Uncertainties for V_{OE} estimated from errors of experimental slope values ($\Delta m = \pm 0.01$) are shown in parentheses.

	N_2/He*($2\,^3S$)	CO/He*($2\,^3S$)	C_2H_2/He*($2\,^3S$)
ζ/Bohr^{-1}	0.498 ($\pm$0.005)	0.584 ($\pm$0.004)	0.510 ($\pm$0.003)
C_1/meV	80 ($\pm$49)	734 ($\pm$44)	98 ($\pm$30)
C_2/meV	9027 ($\pm$71)	8478 ($\pm$58)	6805 ($\pm$27)
C_3/meV	705 ($\pm$23)	495 ($\pm$20)	-470 ($\pm$6)
C_4/meV	88 ($\pm$11)	74 ($\pm$2)	177 ($\pm$8)
C_5/meV	25 ($\pm$2)	57 ($\pm$4)	67 ($\pm$6)
C_6/meV	—	—	48 ($\pm$8)
$K^{(B)}$/eV	6.82	3.35	9.34
$K^{(A)}$/eV	3.72	2.90	11.2
$K^{(X)}$/eV	3.15	1.51	1.43
D_e/meV	-3.09	-6.71	-56.5
R_e/Å	5.35	4.68	2.54
θ_e/degree	35.9	66.4	90.0

for which electron density contour maps are also shown in Figs. 5 and 6. Thick solid curves in the maps indicate the 800 meV contour lines. Since total ionization cross sections cannot be estimated in our calculations, total cross sections for N_2+He*($2\,^3S$) and CO$+$He*($2\,^3S$) were normalized with crossed-beam experiments,[47] and those for C_2H_2 $+$He*($2\,^3S$) were normalized to a reported value.[48] Obtained CEDPICS curves for the OE method by the present trajectory calculations are shown with solid lines.

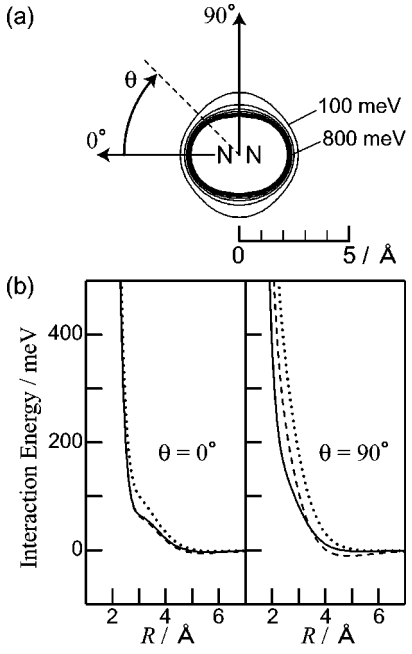

FIG. 2. The potential energy curve for N_2+He*($2\,^3S$) obtained from the OE method (solid line) [see Eq. (5)]. Optimized parameter sets were listed in Table IV. R is the distance between He*($2\,^3S$) and the center-of-mass of N_2, and θ is the angle from the collinear direction. The contour maps for the repulsive boundary positions are shown with an energy spacing of 100 meV. Potential energy curves obtained by the Li model (dotted line) and the EC method (dashed line) are also shown for comparison.

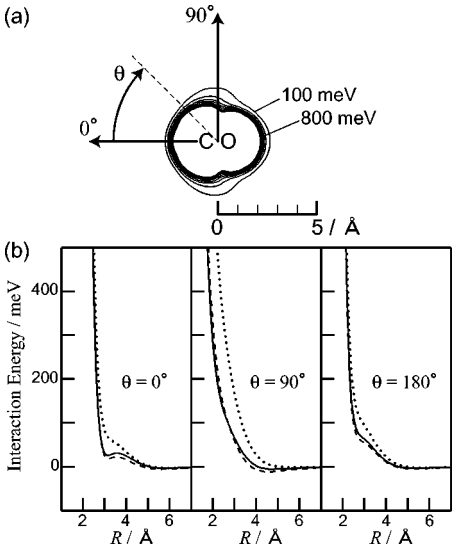

FIG. 3. The potential energy curve for CO+He*($2\,^3S$) obtained from the OE method (solid line) [see Eq. (5)]. Optimized parameter sets were listed in Table IV. R is the distance between He*($2\,^3S$) and the center-of-mass (X) of CO, and θ denotes the CXHe* angle from the collinear direction. The contour maps for the repulsive boundary positions are shown with an energy spacing of 100 meV. Potential energy curves obtained by the Li model (dotted line) and the EC method (dashed line) are also shown for comparison.

V. DISCUSSION

A. Slopes in CEDPICS and modifications of the potentials

As can be seen from Figs. 5 and 6, calculated total and partial Penning ionization cross sections using the present OE model potentials V_{OE} are in excellent agreement with the experiments by 2D-PIES. Table I compares observed and calculated slopes m of $\log \sigma^{(i)}$ versus $\log E_c$ plots for X, A, and B ionic states. Since the SS method is only applicable to repulsive systems, the SS method was not used for C_2H_2. Although relative magnitudes of m are well reproduced by the SS method for N_2 and CO, there are large errors of 0.2–0.4, which cannot be disregarded in comparison with the experimental error bars of *ca.* 0.03. The EC method gave

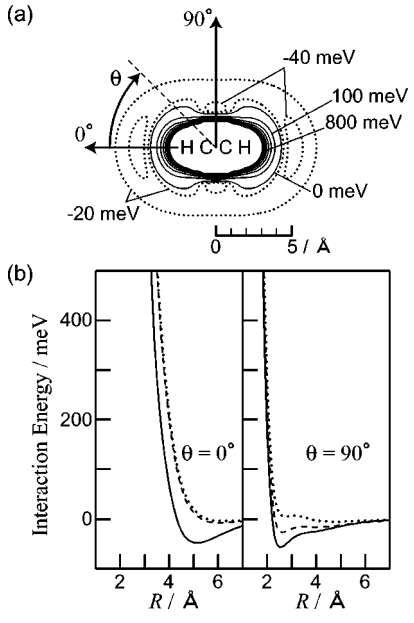

FIG. 4. The potential energy curve for C_2H_2+He*($2\,^3S$) obtained from the OE method (solid line) [see Eq. (5)]. Optimized parameter sets were listed in Table IV. R is the distance between He*($2\,^3S$) and the center-of-mass, and θ is the angle from the collinear direction. The contour maps for the repulsive boundary positions are shown with an energy spacing of 100 meV. For attractive potential wells, contour curves are shown with and energy spacing of 20 meV. Potential energy curves obtained by the EC method (dashed line) are also shown for comparison.

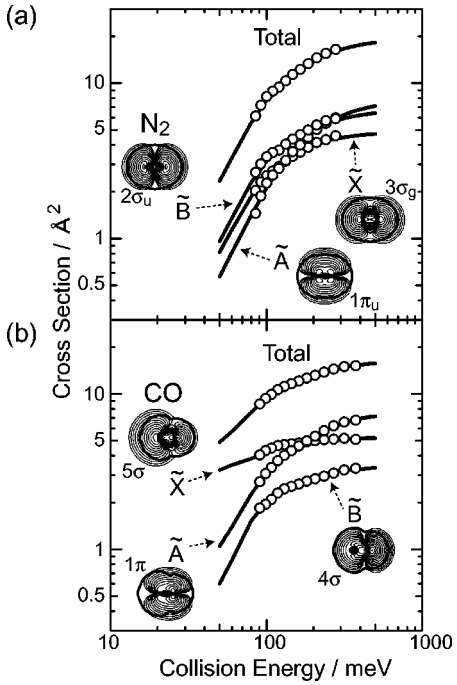

FIG. 5. The $\log \sigma^{(i)}$–$\log E_c$ plots of CEDPICS for (a) N_2+He*($2\,^3S$) and (b) CO+He*($2\,^3S$), respectively. Observed cross sections are plotted with circles. The present calculations are drawn with solid lines. Contour maps of the electron densities for molecular orbitals corresponding to respective ionic states are also shown. Observed total cross sections are normalized to reported values (Ref. 47) at $E_c = 200$ meV.

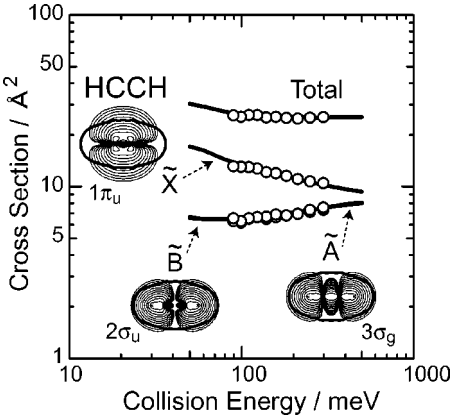

FIG. 6. The $\log \sigma^{(i)}$–$\log E_c$ plots of CEDPICS for C_2H_2+He*($2\,^3S$). Observed cross sections are plotted with circles. Data for the A state are almost overlapped with those for the B state shown beneath. The present calculations are drawn with solid lines. Contour maps of the electron densities for molecular orbitals corresponding to respective ionic states are also shown. Observed total cross sections are normalized to reported values (Ref. 48) at $E_c = 33$ meV.

improved results for N_2 and CO in comparison with those by the SS method. However, the EC method showed the following difficulties. As can be seen in Table I, the slope values at the higher collision energy region for A and B states of N_2 are still considerably different from the observed values. This discrepancy is ascribed to the qualities of potential curves, especially for the perpendicular direction ($\theta=90°$) as shown in Fig. 2; higher energy parts of repulsive wall are still rather soft in comparison with those for the OE curve. In the case of C_2H_2, the EC method gave expansion coefficients (A_0, A_2, and A_4) with very large ranges of uncertainty in Table III. This is probably because the one center expansion of Eq. (4) cannot make sufficient anisotropic corrections. In connection with this, the EC method yielded extremely large K values for C_2H_2, which are one order of magnitude larger than those of other molecules. Since K is a proportionality constant in Eq. (8) for the ionization width, too large values are highly unlikely. Thus, the flexibility of the EC method of Eq. (4) is not sufficient in comparison with the OE method.

B. Characteristic features of potential corrections in the SS and EC methods

Table II shows optimized parameters for the SS method. The values of the scaling factor a for N_2 ($a=0.80$) and CO ($a=0.55$) are much smaller than 1, which indicates that the correct potential for He* should be pulled down to the lower energies from the Li potential V_0. There may be several reasons for this. The larger basis functions as well as the higher levels of electron correlation corrections tend to lower the interaction energies. A careful comparison of various levels of calculations showed that the present V_0 calculations in the CCSD(T)/6-311+G* level is satisfactory. The discrepancy between V_0 and V_{SS} is thus ascribed to intrinsic differences of interactions between M+He* and M+Li. Characteristic features for the K-parameters will be discussed below in comparison with those obtained for the EC and OE methods.

Table III shows optimized parameters for the EC method. As already noted in the previous studies,[38,39] A_2/A_0 has a negative value of *ca.* -0.4 for N_2 and CO, which indicates oblate corrections leading to the more negative contributions pulling down the interaction potentials effectively in the perpendicular directions where π electrons distribute. Therefore, a charge transfer (CT) interaction leading to M^-A^{*+}[49–51] seems to be dominant in the corrections to the Li model potential V_0. This propensity can be understood from the difference of the energy levels between He* and Li atoms. Since the ionization potential of Li($2\,^2S$) (5.392 eV) is larger than that of He*($2\,^3S$) (4.768 eV), the $2s$ electron energy level is much higher for He*. This means that the CT interaction is much more important in He*, because the energy gap between the $2s$ and unoccupied π levels becomes smaller for He*. This argument is consistent with the above propensity for A_2/A_0 values for N_2 and CO. The importance of the CT interaction with target unoccupied orbitals can also be supported by the following aspects on the smaller B parameter. The optimized values for B in Table II are 1.104 Å for N_2 and 0.861 Å for CO, respectively. The characteristic length B in the exponential function can be related with the asymptotic behavior of wave function tail known as $B^{-1}=2(2\mathrm{IP})^{1/2}$, where IP is the ionization potential.[52] The characteristic length of *ca.* 1 Å corresponds to the ionization potential of *ca.* 1 eV which approximately agrees well with the energy level of the unoccupied molecular orbital.

It should be noted that corrections are not necessarily concentrated on the perpendicular sides, because the isotropic term of A_0 in Table II shows large values. Therefore, some other interactions are also responsible for the differences between V_0 and V_{EC}. We should note here that important interactions may involve occupied orbitals of the target molecule as well as the vacant $2p$ orbital in the atom. In this regard, it is very difficult to obtain much more precise information from the EC model.

C. Obtained potential parameters in the OE method and characteristic features

Table IV shows optimized parameter values for the OE method. The optimized ζ values for three systems, 0.498 bohr^{-1} for N_2+Li, 0.584 bohr^{-1} for CO+Li, and 0.510 bohr^{-1} for C_2H_2+Li were found to be very close to the exponent of the $2s$ orbital of He* atom, which is determined to be 0.575 bohr^{-1} by Slater's rule. This indicates that the atomic orbital function χ introduced in Eq. (6) is for the valence $2s$ orbital and not for the inner $1s$ orbital in a He* atom. This is consistent with the approximation replacing a He* atom by a Li atom neglecting the effects of inner orbitals, based on the assumption that the outer electron governs the interactions.

Since the $2s$ electron energy level is much higher for He* ($2\,^3S$) than Li ($2\,^2S$), contributions to energy lowering in the Li potential V_0 are expected to be overestimated for the occupied molecular orbitals and underestimated for unoccupied molecular orbitals. The magnitude of corrections should be the largest for HOMO or LUMO in general because of the smaller energy gaps. Such an argument leads to negative values for the occupied-orbital coefficients and positive values for unoccupied-orbital coefficients.

As can be seen in Table IV, coefficients for unoccupied orbitals, C_4, C_5, and C_6, are really positive, and the magnitude shows a decreasing order from LUMO (C_4) to the higher levels (C_5,C_6). This is consistent with the results for the EC method, which disclosed the CT interaction involving an electron transfer from the atom into the molecule. On the other hand, those for occupied orbitals, C_1, C_2, and C_3, are mostly positive contrary to the above expectation. Moreover, the magnitude is the largest at C_2 for the next HOMO ($1\pi_u$ of N_2, 1π of CO, $3\sigma_g$ of C_2H_2) rather than at C_3 for the HOMO ($3\sigma_g$ of N_2, 5σ of CO and $1\pi_u$ of C_2H_2).

It should be noted here that the $2s$ unpaired electron in the singly occupied orbital has an antibonding character in the interacting system. In connection with this, contributions of vacant $2p$ orbitals to $2s-2p$ hybridization in the outer shell of the He*(Li) atom should be considered;[10,23,53–56] when the extent of $2s-2p$ hybridization increases, the electron overlap repulsion with the target molecule decreases because of the small lobe of the $2s-2p$ hybridization. Thus,

the $2s-2p$ hybridization contributes also to the energy lowering. However, its magnitude considerably increases in He*, because the $2s-2p$ energy gap becomes much smaller in He* than in Li; the energy gap between $2s$ and $2p$ orbital of He*($2\,^3S$) (1.114 eV) is much smaller than that of Li ($2\,^2S$) (1.848 eV). This indicates that the Li model potentials seriously underestimate the $2s-2p$ hybridization effect and thus overestimate overlap repulsions.

Since the $2s-2p$ mixing occurs via interactions with occupied molecular orbitals, correction terms for occupied molecular orbitals can be positive, when the $2s-2p$ hybridization effect pulling down the unpaired electron level is much more important than the lowering effects on the paired electron levels for the occupied molecular orbitals. The positive signs for the occupied-orbital coefficients in Table IV clearly indicate that the $2s-2p$ hybridization effect dominates. Although the magnitude of the coefficients for the occupied orbitals is not the highest at HOMO, this may be caused by cancellation with the negative sign contributions from the interactions of paired electrons. This cancellation effect of paired electrons is expected to be largest in the HOMO levels, especially in the case of C_2H_2, since the ionization potential for the HOMO of C_2H_2 is 11.40 eV, which is much smaller than those for CO (14.01 eV) and N_2 (15.60 eV). This order is consistent with the increasing order of the coefficient C_3 for HOMO, -470 for C_2H_2, 495 for CO, and 705 for N_2. A similar tendency depending on the energy gaps can also be found for the next-HOMO coefficient C_2.

These findings show that on going from the larger IP to the smaller IP of target molecules the major contribution to the energy lowering mechanisms involving occupied electrons changes from the $2s-2p$ hybridization effect to the interactions between the target electron pairs and the atomic unpaired electron. This is consistent with a propensity in elastic scattering data,[35] for which attractive potential wells of interactions with atomic targets having small ionization potentials such as alkali metal atoms have been found to be deeper for Li rather than for He*.

Although expansion coefficients C_i for interactions between the $2s$, orbital of He* and unoccupied molecular orbitals were found to be much smaller than those for interactions between the $2s$ orbital of He* and occupied molecular orbitals, corrections due to unoccupied molecular orbitals are very important at relatively long distances where the other types of interactions are very small. Therefore, the CT interactions involving unoccupied molecular orbitals are of great significance at longer distances.

In connection with the above findings, it is worthy to compare well-depths D_e and well-positions R_e and θ_e in Table IV. In the case of N_2 and CO, ionization potentials are so high that energy lowering interactions leading to potential wells are only effective in long distances, where unoccupied molecular orbitals are relevant for the CT interactions. The obtained angles θ_e for N_2 ($\theta_e=35.9°$) and CO ($\theta_e=66.4°$) are related with electron distributions of unoccupied orbitals ϕ_4 and ϕ_5 shown in Fig. 1 in the present OE method, though the EC methods gave much larger angles for N_2 ($\theta_e=90°$) and CO ($\theta_e=80.3°$). The parameters for N_2 ($D_e=3.09$ eV, $R_e=5.35$ Å) in the OE method gave much better agreement with those obtained by scattering experiments ($D_e=ca.\ 2$ meV, $R_e=5.7$ Å)[57] than the EC method. In the case of C_2H_2, the ionization potential becomes small enough to have a strong interaction between occupied π orbitals and the He* atom. Thus the location of the potential well is around the perpendicular direction ($\theta_e=90°$) at a relatively short distance of $R_e=2.54$ Å, where occupied π orbitals have large electron densities. The well positions for C_2H_2 by the OE method agree well with those by the EC method, though the depth is considerably different. The well depths of $D_e=56.5$ meV for C_2H_2 is much larger than those for N_2 and CO, and hence the slope m of $\log\sigma^{(i)}$–$\log E_c$ plots for the X state (corresponding to the $1\pi_u$ orbital) of C_2H_2 has negative values of *ca.* -0.2 due to the attractive interactions, whereas for other ionic states the slope values m are positive reflecting repulsive potentials, as can be seen in Table I and Fig. 4.

D. Parameter fitting for the ionization width

In connection with the optimization of potential functions, parameters $K^{(i)}$ for the overlap method evaluating ionization widths in Eq. (8) were optimized. As can be seen from Tables II–IV, obtained values for $K^{(i)}$ have some interesting features. Absolute values are different among the SS, EC, and OE methods, while the relative magnitudes for three ionic states in each system are rather similar. Since ionization cross sections depend on both interaction potentials and ionization width, K-parameters may be affected by qualities of interaction potentials via the optimization processes. In the case of N_2 and CO, magnitudes of $K^{(i)}$ showed relative orders of SS>EC,OE. This propensity is consistent with the magnitudes of potential energy lowering in these methods mentioned above. In the SS method, insufficient potential energy lowering caused substantial increases of the K-parameter values.

Another tendency in the magnitudes of the K-parameters, $K^{(B)}>K^{(A)}>K^{(X)}$, were found for the relative orders among the ionic states. This tendency may be related to a factor of $E_e^{-1/2}$ involved in a formula for the ionization width.[58] The energy gap between the He $1s$ orbital and the target ionized orbital may also be responsible for this tendency in connection with the electron transfer matrix elements as discussed in the previous study.[39] It seems to be important that the K values for A and B states of C_2H_2 are still rather large even in the OE method. Although this may be due to some inaccuracies in the interaction potentials, we should point out that electron correlation effects are not included in the calculations of the ionization widths. The mixing of higher vacant orbitals with the same symmetry of the ionized occupied orbital may possibly contribute strong enhancements of the ionization widths. If the vacant $4\sigma_g$ and $3\sigma_u$ orbitals are mixed into occupied $3\sigma_g$ and $2\sigma_u$ orbitals, respectively, electron densities may substantially increase in the exterior regions to result in enhanced ionization cross sections.

E. Characteristic remarks of the overlap expansion method

In the present study we demonstrate the following features of the overlap expansion (OE) method for corrections of approximate interaction potentials:

(1) Overestimation or underestimation of important orbital interactions between interacting species involved in the approximate interaction potentials to be optimized can be improved effectively and efficiently.

(2) From the sign and the magnitude of each expansion coefficient, deficiencies involved in the approximate interaction potentials can be clarified.

(3) Correction terms can be limited to valence orbitals. Major contributions are expected for HOMO, LUMO, next-HOMO, and next-LUMO, because of the energy gap law for orbital interactions.

(4) Highly anisotropic interactions intrinsic to the molecules can be considered effectively, because most parts of anisotropic interactions are essentially related to spatial characteristics of molecular orbitals.

(5) In connection with the above features (3) and (4), the number of correction terms can be suppressed to be small, even if the size of the molecular system becomes large.

Although the exponential correction (EC) method using exponential terms with Legendre expansions gave nearly the same qualities of interaction potentials after optimization as the present OE method in the case of CO, the following remarks should be noted. None of the above mentioned features for the OE method from (2)–(5) could be obtained for the EC method. Even for the feature (1), the EC method will have serious difficulties if it is applied to nonlinear molecules or very large molecules. Because of the one-center-scheme of the Legendre expansion, too many terms should be contained for highly anisotropic systems. This is crucial, since intermolecular interactions are highly anisotropic and essentially very local. This kind of drawbacks can also be expected for many other techniques using limited shape of expansion terms, such as van der Waals terms or multipole expansions.

The reason why the present OE method works efficiently can be explained as follows. In quantum theories of molecular systems, the fundamental equation for the total electronic energy is made up of one electron core integrals and two electron repulsion integrals. It has been well known that in many semi-empirical theories these integrals can be approximated by using overlap integrals between the orbitals included in the integral.[59] Although these approximations becomes less accurate in a very short distance, electron transfer[60] or electron exchange processes as well as exciton diffusion processes[61] have been smiepirically treated with this sort of approximations. Even for including electron correlations, the correction terms can be expanded into one or two electron integrals which are then approximated by using overlap integrals. Thus, correction of intermolecular potentials can be made in terms of overlap integrals between orbitals of the interacting systems. In the present study, the expansion coefficients in the OE method were treated as constants irrespective of the geometrical configurations of the interacting systems. This treatment enables us to optimize complex features of interaction potentials efficiently with limited computational efforts.

Applications of the present OE method to other systems, such as OCS[62] and C_6H_6[63] with $He^*(2\,^3S)$, have been found to be successful. These results will be published elsewhere.

VI. CONCLUSION

An overlap expansion (OE) method was proposed for improving intermolecular interaction potentials. Correction terms were introduced as a linear combination of squares of overlap integrals between interacting species, in order to include highly anisotropic interactions intrinsic to the molecular systems. The present OE method was applied to improve crude potentials for intermolecular interactions between a molecule (N_2, CO, C_2H_2) and a metastable atom [$He^*(2\,^3S)$]. The crude potentials using a $Li(2\,^2S)$ atom in place of a $He^*(2\,^3S)$ atom based on their qualitative similarity were improved very efficiently; an overestimation and underestimation of important orbital interactions in the crude potentials were corrected for individual valence orbitals, such as HOMO and LUMO. From the sign and the magnitude of the expansion coefficients, deficiencies in the crude potentials are elucidated in terms of orbital interactions. Since the number of correction terms can be limited to be small for certain important valence orbitals, the present OE method is highly promising for its application to large molecules, for which other methods will meet with computational difficulties arising from too many parameters and their indeterminacy.

ACKNOWLEDGMENTS

The present work was supported partly by a Grant-in-Aid for Scientific Research from the Japanese Ministry of Education, Science, and Culture. M.Y. is supported by the Research Fellowship of the Japan Society for the Promotion of Science for Young Scientists.

[1] J. N. Murrel, S. Carter, S. C. Farantos, P. Huxley, and A. Varandas, *Molecular Potential Energy Functions* (Wiley, Chichester, 1984).
[2] G. C. Schatz, Rev. Mod. Phys. **61**, 669 (1989).
[3] A. F. Sax, in *Potential Energy Surfaces: Proceedings of the Mariapfarr Workshop in Theoretical Chemistry* (Springer-Verlag, Berlin, 1999).
[4] A. J. Stone, *The Theory of Intermolecular Forces* (Oxford University Press, Oxford, 1996).
[5] S. Scheiner, in *Molecular Interactions: From van der Waals to Strongly Bound Complexes* (Wiley, Chichester, 1997).
[6] A. J. Yencha, in *Electron Spectroscopy: Theory, Techniques and Applications*, edited by C. R. Brundle and A. D. Baker (Academic, New York, 1984), Vol. 5.
[7] H. Hotop and A. Niehaus, Z. Phys. **228**, 68 (1969).
[8] A. Niehaus, Adv. Chem. Phys. **45**, 399 (1981).
[9] K. Mitsuke, T. Takami, and K. Ohno, J. Chem. Phys. **91**, 1618 (1989).
[10] K. Ohno, T. Takami, K. Mitsuke, and T. Ishida, J. Chem. Phys. **94**, 2675 (1991).
[11] T. Takami, K. Mitsuke, and K. Ohno, J. Chem. Phys. **95**, 918 (1991).
[12] T. Takami and K. Ohno, J. Chem. Phys. **96**, 6523 (1992).
[13] D. C. Dunlavy, D. W. Martin, and P. E. Siska, J. Chem. Phys. **93**, 5347 (1990).
[14] E. J. Longley, D. C. Dunlary, H. M. Bevsek, and P. E. Siska, J. Phys. Chem. **97**, 2097 (1993).
[15] D. C. Dunlavy and P. E. Siska, J. Phys. Chem. **100**, 21 (1996).

[16] K. Ohno, H. Yamakado, T. Ogawa, and T. Yamata, J. Chem. Phys. **105**, 7536 (1996).
[17] H. Nakamura, J. Phys. Soc. Jpn. **26**, 1473 (1969).
[18] W. H. Miller, J. Chem. Phys. **52**, 3563 (1970).
[19] R. E. Olson, Phys. Rev. A **6**, 1031 (1972).
[20] N. T. Padial, R. L. Martin, J. S. Cohen, and N. F. Lane, Phys. Rev. A **39**, 2715 (1989).
[21] A. Merz, M. W. Muller, M.-W. Ruf, H. Hotop, W. Mayer, and M. Movre, Chem. Phys. **145**, 219 (1990).
[22] M. Kimura and N. F. Lane, Phys. Rev. A **41**, 5938 (1990).
[23] J. S. Cohen and N. F. Lane, J. Chem. Phys. **66**, 586 (1977).
[24] A. P. Hickman, A. D. Isaacson, and W. H. Miller, J. Chem. Phys. **66**, 1483 (1977).
[25] D. C. Dunlavy and P. E. Siska, J. Phys. Chem. **100**, 21 (1996).
[26] T. Ishida, Chem. Phys. Lett. **211**, 1 (1993).
[27] T. Ishida and K. Horime, J. Chem. Phys. **105**, 5380 (1996).
[28] T. Ishida, Chem. Phys. Lett. **191**, 1 (1992).
[29] T. Ogawa and K. Ohno, J. Chem. Phys. **110**, 3773 (1999).
[30] E. W. Rothe, R. H. Neynaber, and S. Trujillo, J. Chem. Phys. **42**, 3310 (1965).
[31] H. Hotop, Radiat. Res. **59**, 379 (1974).
[32] E. E. Mouschlitz, Jr., Science **159**, 599 (1968).
[33] W. H. Miller and H. F. Schaefer, III, J. Chem. Phys. **53**, 1421 (1970).
[34] H. Haberland, Y. T. Lee, and P. E. Siska, Adv. Chem. Phys. **45**, 487 (1981).
[35] H. Hotop, T. E. Roth, M.-W. Ruf, and A. J. Yencha, Theor. Chem. Acc. **100**, 36 (1998).
[36] K. Ohno, M. Yamazaki, N. Kishimoto, T. Ogawa, and K. Takeshita, Chem. Phys. Lett. **332**, 167 (2000).
[37] M. Yamazaki, N. Kishimoto, M. Kurita, T. Ogawa, K. Ohno, and K. Takeshita, J. Electron Spectrosc. Relat. Phenom. **114–116**, 175 (2001).
[38] M. Yamazaki, S. Maeda, N. Kishimoto, and K. Ohno, Chem. Phys. Lett. **355**, 311 (2002).
[39] M. Yamazaki, S. Maeda, N. Kishimoto, and K. Ohno, J. Chem. Phys. **117**, 5707 (2002).
[40] S. F. Boys, F. Bernardi, Mol. Phys. **19**, 553 (1970).
[41] M. J. Frisch, G. W. Trucks, H. B. Schlegel *et al.*, GAUSSIAN 94, Revision C.3, Gaussian, Inc., Pittsburgh, PA, 1995.
[42] W. H. Press, S. A. Teukolsky, W. T. Vetterling, and B. P. Flannery, *Numerical Recipes in C* (Cambridge University Press, Cambridge, 1988).
[43] M. J. D. Powell, Computer J. **7**, 303 (1965).
[44] N. Kishimoto, M. Furuhashi, and K. Ohno, J. Electron Spectrosc. Relat. Phenom. **88–91**, 143 (1998).
[45] J. L. Gardner and J. A. R. Samson, J. Electron Spectrosc. Relat. Phenom. **8**, 469 (1976).
[46] K. Kimura, S. Katsumata, Y. Achiba, T. Yamazaki, and S. Iwata, *Handbook of* He I *Photoelectron Spectra of Fundamental Organic Molecules*, Japan Scientific, Tokyo, 1981.
[47] T. P. Parr, D. M. Parr, and R. M. Martin, J. Chem. Phys. **76**, 316 (1982).
[48] T. Ueno, Y. Hatano, Oyo Butsuri **47**, 1006 (1978).
[49] J. L. Magee, J. Chem. Phys. **8**, 687 (1940).
[50] V. Aquilanti, D. Cappelletti, and F. Pirani, Chem. Phys. Lett. **271**, 216 (1997).
[51] B. Brunetti, P. Candori, J. De Andres, F. Pirani, M. Rosi, S. Falcinelli, and F. Vecchiocattivi, J. Phys. Chem. A **101**, 7505 (1997).
[52] J. Katriel and E. R. Davidson, Proc. Natl. Acad. Sci. U.S.A. **77**, 4403 (1980).
[53] A. D. Issacson, A. P. Hichman, and W. H. Miller, J. Chim Phys. **67**, 370 (1977).
[54] P. E. Siska, Chem. Phys. Lett. **63**, 25 (1979).
[55] P. E. Siska, J. Chem. Phys. **71**, 3942 (1979).
[56] D. W. Martin and P. E. Siska, J. Chem. Phys. **82**, 2630 (1985).
[57] H. Hotop, E. Kolb, and J. Lorenzen, J. Electron Spectrosc. Relat. Phenom. **16**, 213 (1979).
[58] W. H. Miller, C. A. Slocomb, and H. F. Schaefer, III, J. Chem. Phys. **56**, 1347 (1972).
[59] R. S. Mulliken, J. Chem. Phys. **46**, 497 (1949).
[60] Vu. N. Demikov, Sov. Phys. JETP **18**, 138 (1964).
[61] S.-I. Choi, J. Jortner, S. A. Rice, and R. Silbey, J. Chem. Phys. **41**, 3294 (1964).
[62] N. Kishimoto, T. Horio, S. Maeda, and K. Ohno, Chem. Phys. Lett. **379**, 332 (2003).
[63] M. Yamazaki, S. Maeda, and K. Ohno, Chem. Phys. Lett. (to be published).